# Supporting Information

## A $CoSe_2$-based 3D conductive network for high-performance potassium storage: enhancing charge transportation by encapsulation and restriction strategy

Jing Zhao [a] †, Hu Wu [a] †, Long Li [a], Shiyao Lu [b], Heng Mao [a], Shujiang Ding [a] *

[a] *School of Chemistry, Xi'an Key Laboratory of Sustainable Energy Materials Chemistry, State key laboratory of Electrical Insulation and Power Equipment, Department of Applied Chemistry, Xi'an Jiaotong University & Shaanxi Quantong Joint Research Institute of New Energy Vehicles Power, Xi'an Jiaotong University, Xi'an 710049, China*

[b] *Department of Chemistry, City University of Hong Kong, Hong Kong, China*

* Corresponding authors

E-mail: dingsj@mail.xjtu.edu.cn

† J. Zhao and H. Wu contributed equally to this work.

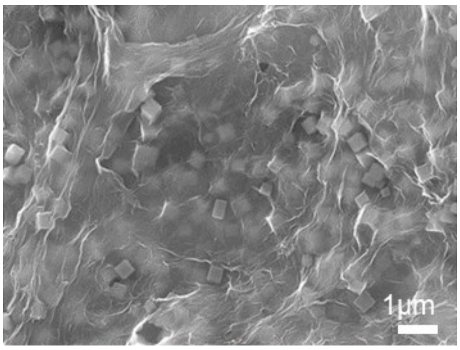


**Figure S1** SEM image of CoCoPBA/GO-2

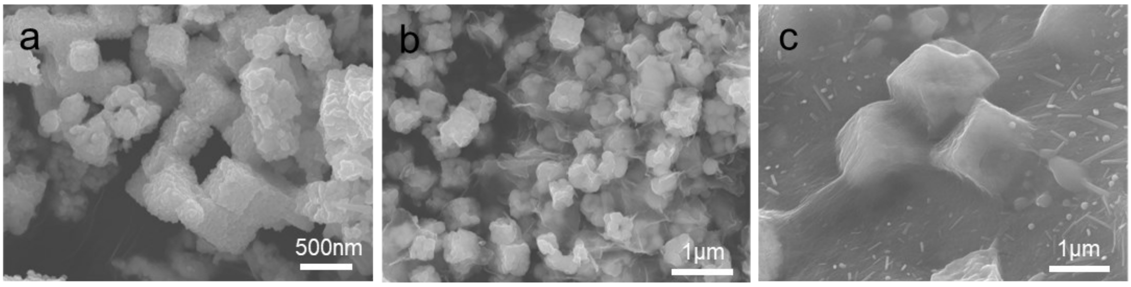


**Figure S2** SEM image of (a) $CoSe_2$@NC (b) $CoSe_2$@NC/rGO-1 and (c) $CoSe_2$@NC/rGO-10.

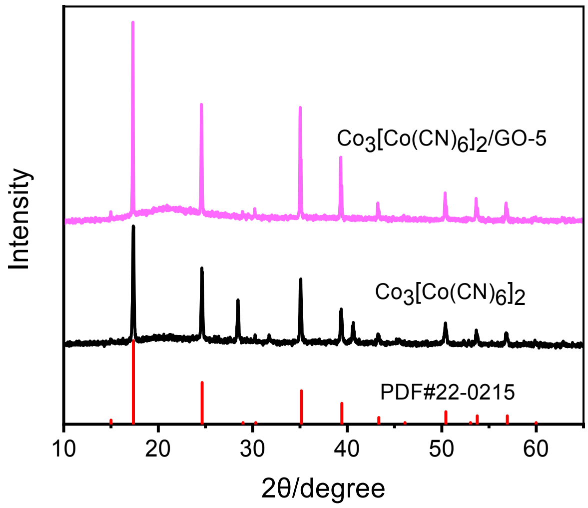


**Figure S3** XRD pattern of the $Co_3[Co(CN)_6]_2$ and $Co_3[Co(CN)_6]_2$/GO-5.

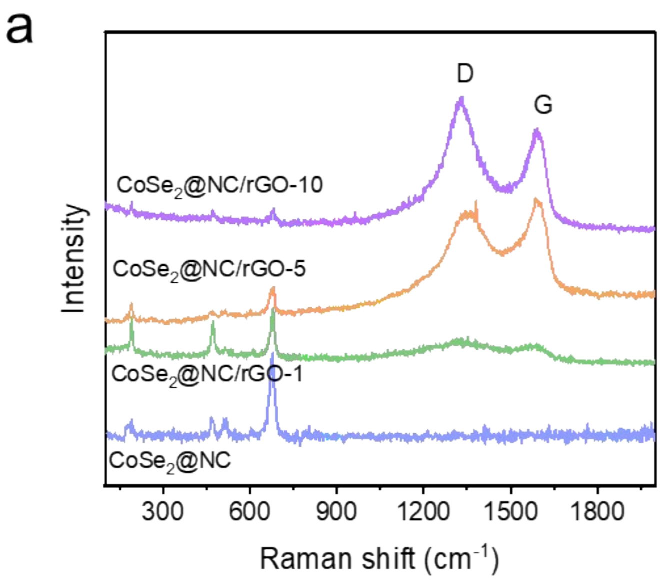


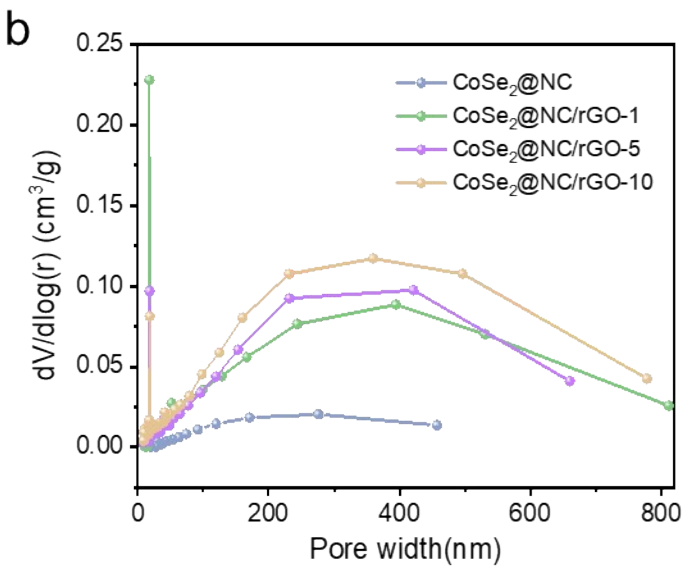


**Figure S4** (a) Raman spectra and (b) pore size distribution of $CoSe_2$@NC, $CoSe_2$@NC/rGO-1, $CoSe_2$@NC/rGO-5 and $CoSe_2$@NC/rGO-10.

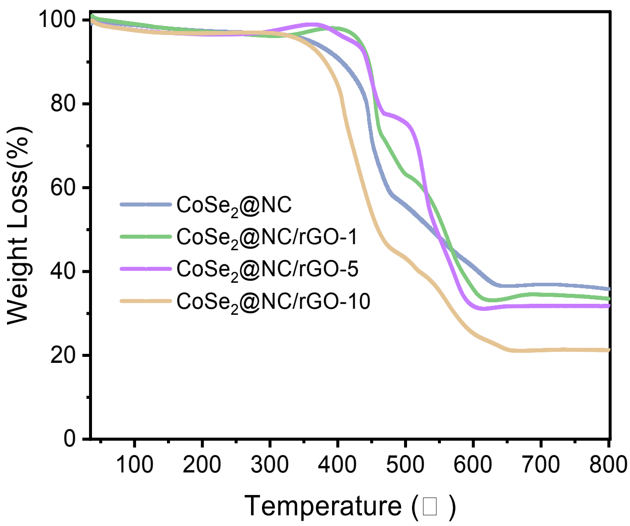


**Figure S5** Normalized remaining mass measured by TGA analysis Raman spectra of $CoSe_2$@NC, $CoSe_2$@NC/rGO-1, $CoSe_2$@NC/rGO-5 and $CoSe_2$@NC/rGO-10.

The weight percentage of $CoSe_2$ in $CoSe_2$@NC and $CoSe_2$@NC/rGO composites was determined by thermogravimetry (TGA) in an oxygen atmosphere at a heating rate of 10 °C min$^{-1}$ from 35 to 800 °C, as shown in **Figure S4**. It can be seen that the samples show one-step weight gain and multi-step weight loss. The small mass loss below 200 °C is attributed to the evaporation of adsorbed water. The main mass loss between 200 and 800 °C is attributed to the oxidation of $CoSe_2$ and the combustion of carbon.

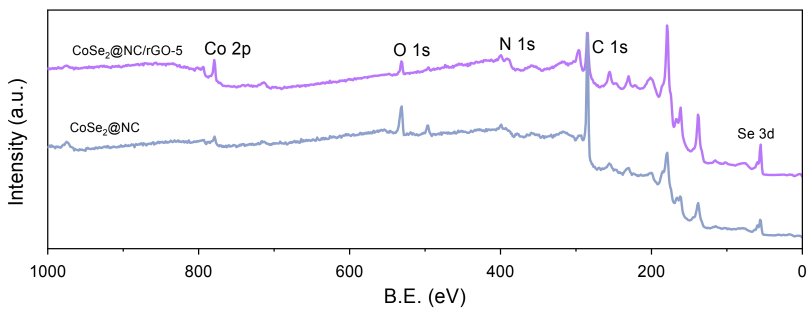


**Figure S6** XPS spectra of $CoSe_2$@NC and$CoSe_2$@NC/rGO-5.

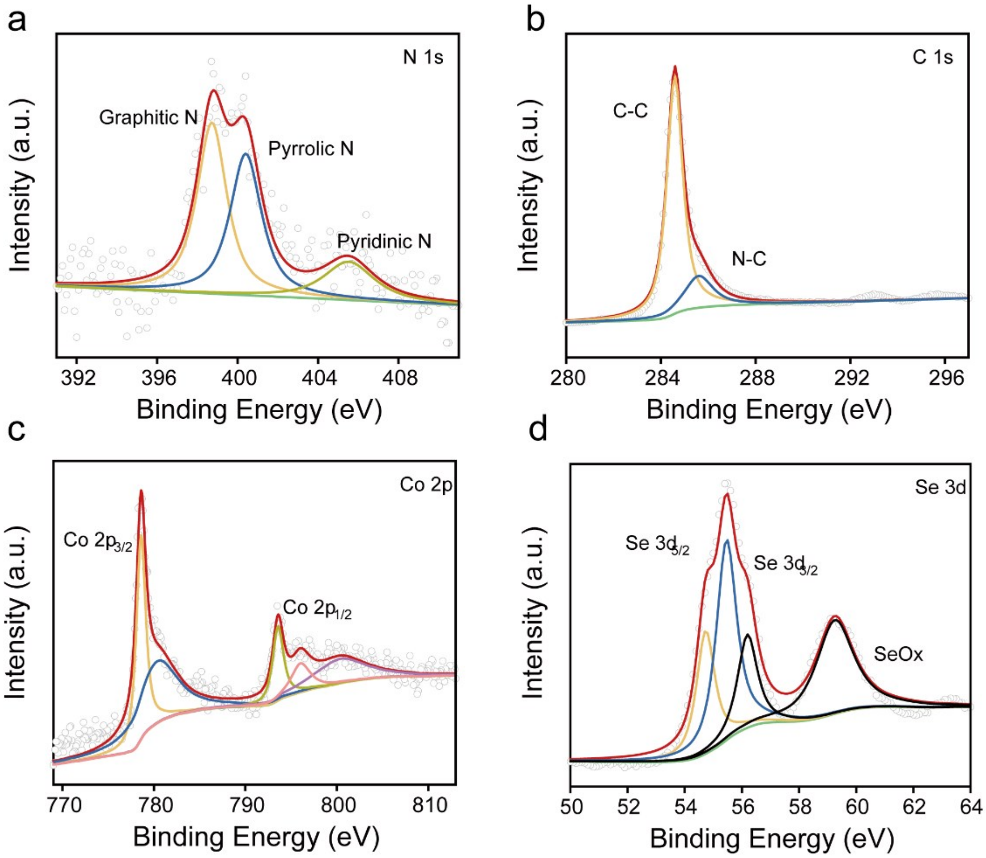


**Figure S7** XPS spectra of $CoSe_2$@NC (a) N 1s, (b) C 1s, (c) Co 2p, and (d) Se 3d.

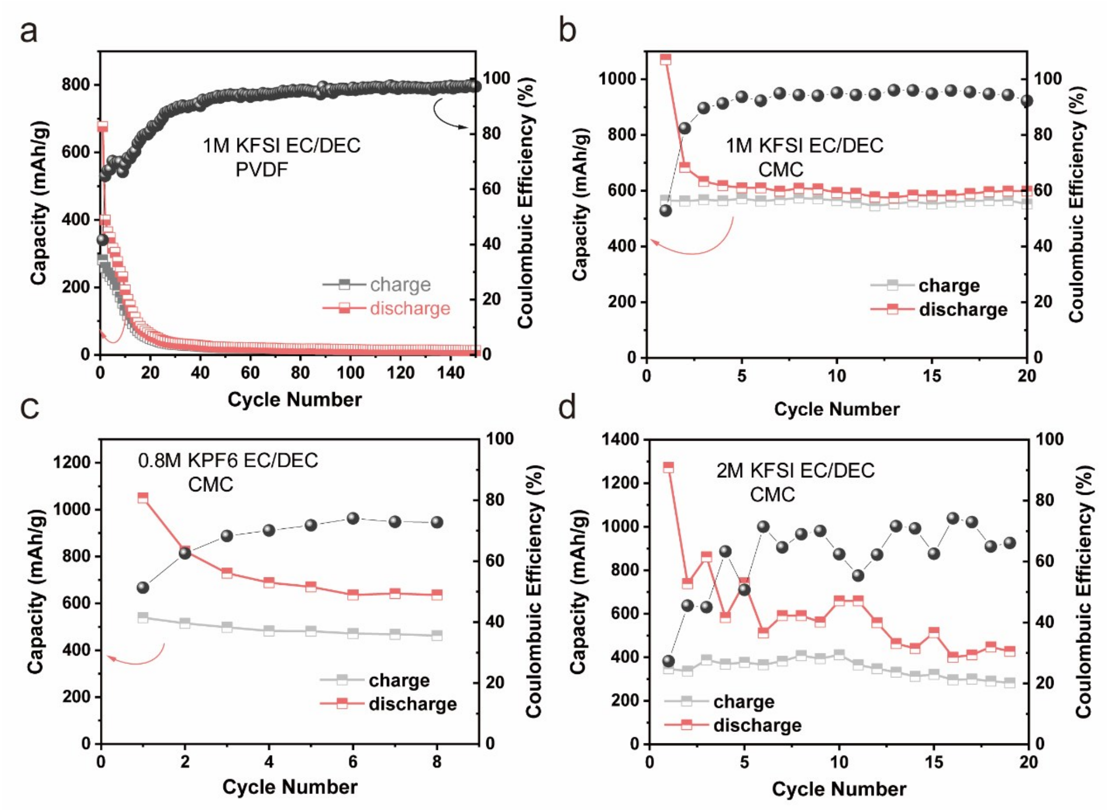


**Figure S8** Cycling performance of $CoSe_2$@NC electrodes at a current density of 0.1 A $g^{-1}$ (a) PVDF (b) CMC as binder, 1M KFSI EC/DEC (v/v=1:1) as electrolyte; (c) CMC as binder, 0.8 M $KPF_6$ EC/DEC (v/v=1:1) (d) CMC as binder, 2M KFSI EC/DEC (v/v=1:1) as electrolyte.

As the potassium ion battery is not yet mature, in order to select the appropriate adhesive and electrolyte, PVDF, CMC were used as the adhesive, 0.8M $KPF_6$ EC/DEC (v/v, 1:1), 1M KFSI EC/DEC (v/v, 1:1) and 2M KFSI EC/DEC (v/v, 1:1) as the electrolyte respectively, and $CoSe_2$@NC/rGO-5 was tested under the current density of 100mA $g^{-1}$. From **Figure S8a**, it can be seen that the specific capacity of $CoSe_2$@NC/rGO-5 with PVDF as binder rapidly decays to zero at the current density of 100mA $g^{-1}$, and the coulomb efficiency is less than 90%. However, $CoSe_2$@NC/rGO-5 with CMC as binder has stable cycle performance and high coulomb efficiency (**Figure S8b**). This may be due to the formation of a uniform passivation layer on the surface of the material by CMC binder[1]. The hydrogen bond formed by a large number of hydroxyl groups in CMC has a strong adhesion, inhibiting the shedding of active substances[1]. Therefore, CMC is more suitable as the binder of $CoSe_2$@NC/rGO-5 electrode material.

It is impressive that 1M KFSI EC/DEC electrolyte has higher stability and coulomb efficiency than the other two electrolytes (**Figure S8b-d**). This is because in the traditional $KPF_6$ EC/DEC electrolyte system, the volume of the negative electrode material changes dramatically during the charging and discharging process, which destroys the existing SEI film, thus constantly consuming the electrolyte to produce new SEI, resulting in rapid capacity degradation. On the contrary, under the condition of same solvent, the SEI produced by replacing $KPF_6$ salt with KFSI salt has a good stability, which can effectively reduce the side reactions and alleviate the capacity degradation caused by the volume change of negative materials. In 2M KFSI EC/DEC (v/v, 1:1) electrolyte, the high concentration of KFSI has a great influence on the mobility of potassium ions in the battery. Therefore, the suitable adhesive and electrolyte for $CoSe_2$@NC/rGO-5 are CMC and 1M KFSI EC/DEC (V / V, 1:1), respectively.

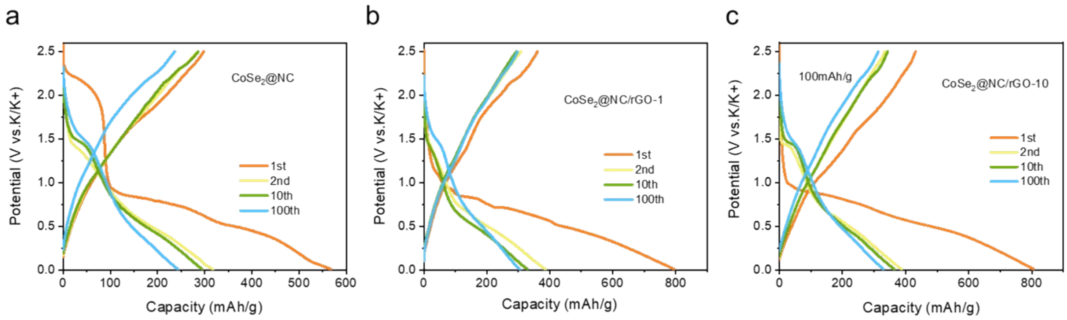


**Figure S9** Charge/discharge profiles of (a) $CoSe_2$@NC, (b) $CoSe_2$@NC/rGO-1 and (c) $CoSe_2$@NC/rGO-10 electrodes at a scan rate of 0.1 mV $s^{-1}$ at the 1st, 2nd, 10th and 100th cycles.

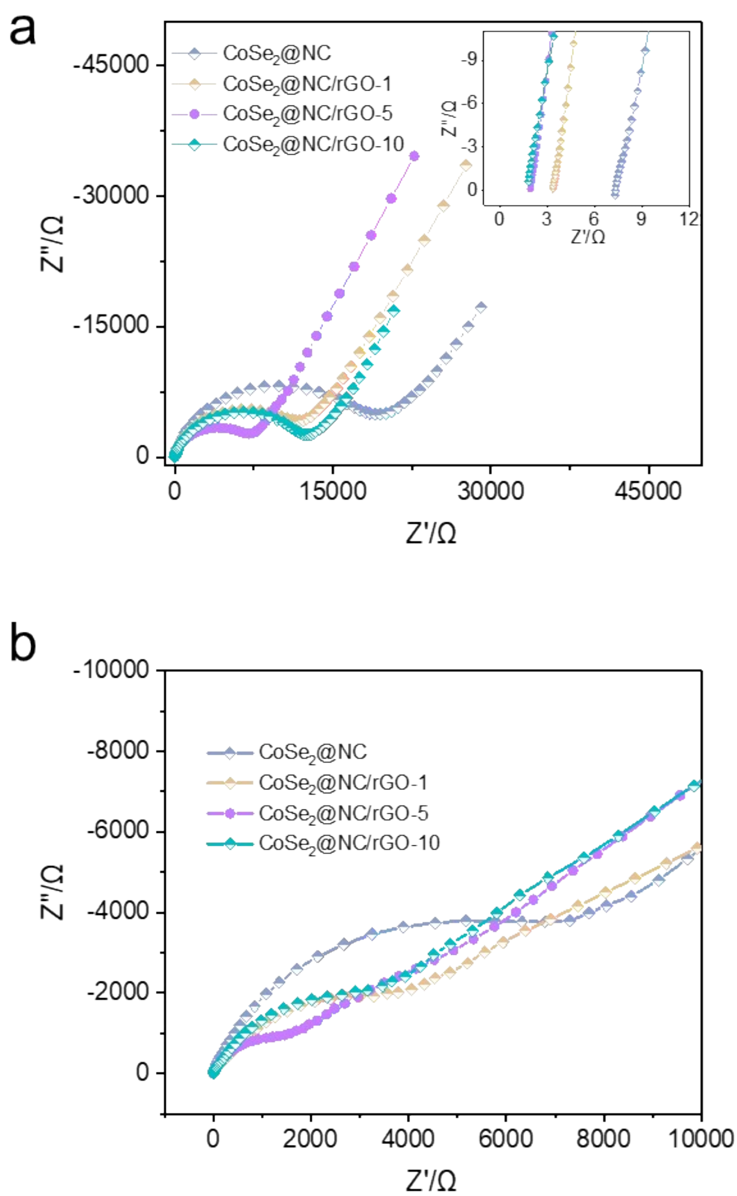


**Figure S10** Nyquist plots of the $CoSe_2$@NC, $CoSe_2$@NC/rGO-1, $CoSe_2$@NC/rGO-5 and $CoSe_2$@NC/rGO-10 electrodes at OCV (a) and after 50 cycles (b). The inset depicts the intercepts of the four EIS spectra with Z' axis.

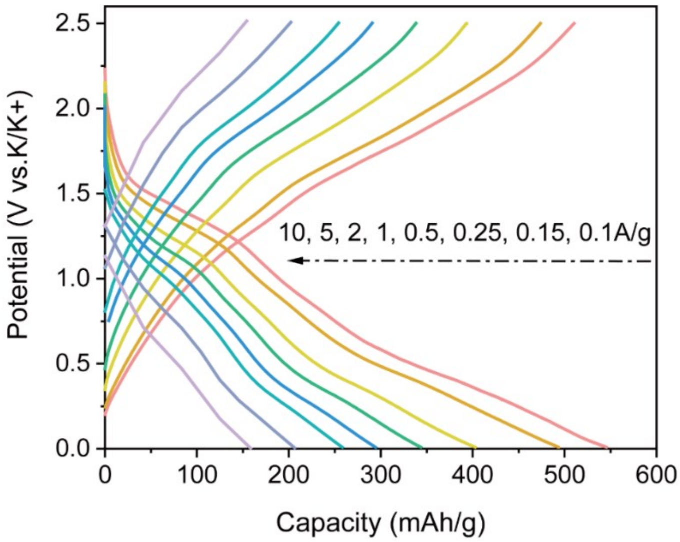


**Figure S11** Charge/discharge curves of the $CoSe_2$@NC/rGO-5 electrode at various current densities.

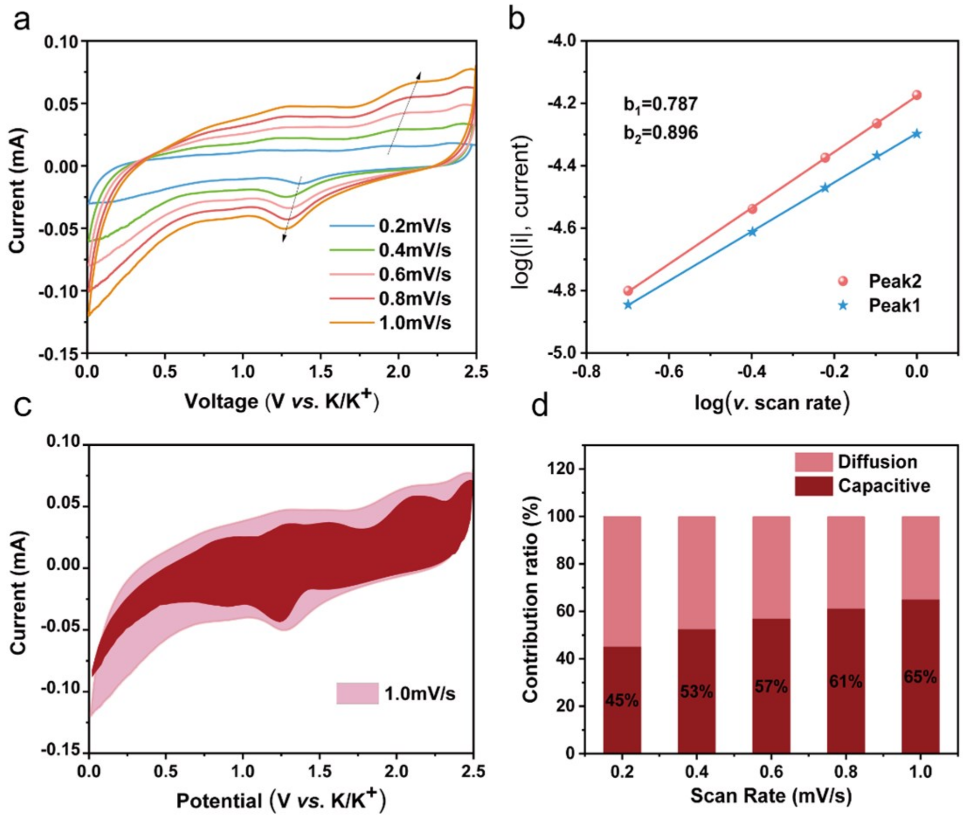


**Figure S12** (a) The cyclic voltammograms of the $CoSe_2$@NC electrode at various scan rates; (b) Determination of the b value using the relationship between peak current and scan rate; (c) Separation of the capacitive current in the $CoSe_2$@NC electrode at a scan rate of 1.0 mV $s^{-1}$ with the capacitive fraction shown by the shaded region; (d) Relative contribution of the capacitive and diffusion-controlled charge storage at different scan rates.

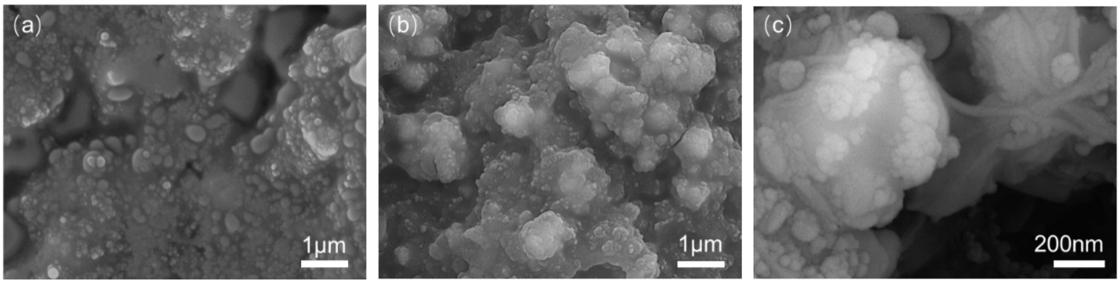


**Figure S13** SEM image of (a) $CoSe_2$@NC and (b,c) $CoSe_2$@NC/rGO-5 electrodes after 5 cycles.

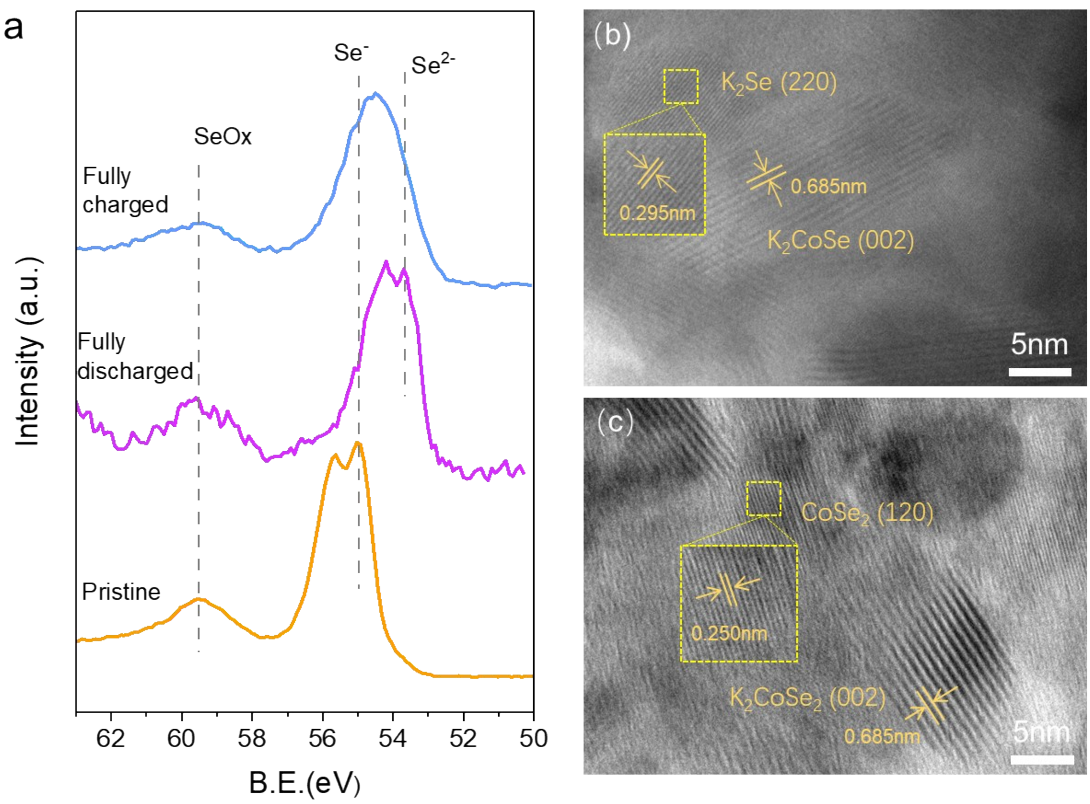


**Figure S14** *Ex-situ* XPS data of (a) Se 2p peaks for pristine, fully discharged and fully charged $CoSe_2$@NC/rGO-5, HRTEM images of the fully discharged (b), fully charged (c) $CoSe_2$@NC/rGO-5 electrodes after 5 cycles.

**Table S1** the electronic conductivity of $CoSe_2$@NC/rGO-x electrode by four-probe method

| Samples | $CoSe_2$@NC electrode ($10^5$ S/cm) | $CoSe_2$@NC/RGO-5 electrode ($10^6$ S/cm) |
|---|---|---|
| **1** | 2.2567 | 4.6865 |
| **2** | 2.4785 | 4.8027 |
| **3** | 2.3768 | 4.5515 |
| **Average** | 2.3767 | 4.6802 |

**Table S2** Comparison of electrochemical cycle performance of $CoSe_2$@NC/rGO with other reported anodes

| Anode | Cycle number | Discharge capacity (mAh $g^{-1}$) | Current density (mA $g^{-1}$) | Reference |
|---|---|---|---|---|
| Yolk–Shell $FeS_2$@C | 40 | 400 | 150 | [2] |
| spherical $MoSe_2$/N-doped carbon | 300 | 258 | 100 | [3] |
| $VS_2$ nanosheet assemblies | 60 | 410 | 100 | [4] |
| Nanosheets-Assembled CuSe Crystal Pillar | 40 | 337 | 200 | [5] |
| $SnS_2$/Graphene nanocomposite | 50 | 610 | 50 | [6] |
| Metallic Graphene-Like $VSe_2$ Ultrathin Nanosheets | 200 | 335 | 200 | [7] |
| $FeS_2$ hollow nanocages@rGO | 50 | 300 | 50 | [8] |
| Flexible $ReS_2$ nanosheets/N-doped carbon nanofibers | 100 | 253 | 50 | [9] |
| SnS@C/rGO | 30 | 375 | 100 | [10] |
| N-doped graphene/$ReSe_2$/$Ti_3C_2$ MXene | 5 | 395.3 | 100 | [11] |
| $MoSe_2$@10%rGO | 50 | 314.0 | 100 | [12] |
| $CoSe_2$@NC/rGO-5 | 100 | 521 | 100 | This work |

## Reference


1. J. Li; N. Zhuang; J. Xie; Y. Zhu; H. Lai; W. Qin; M. S. Javed; W. Xie; W. Mai, Carboxymethyl Cellulose Binder Greatly Stabilizes Porous Hollow Carbon Submicrospheres in Capacitive K-Ion Storage. *ACS Appl Mater Interfaces* 2019, ***11*** (17), 15581-15590.
2. Y. Zhao; J. Zhu; S. J. H. Ong; Q. Yao; X. Shi; K. Hou; Z. J. Xu; L. Guan, High-Rate and Ultralong Cycle-Life Potassium Ion Batteries Enabled by In Situ Engineering of Yolk-Shell $FeS_2$@C Structure on Graphene Matrix. *Advanced Energy Materials* 2018, ***8*** (36).
3. J. Ge; L. Fan; J. Wang; Q. Zhang; Z. Liu; E. Zhang; Q. Liu; X. Yu; B. Lu, $MoSe_2$/N-Doped Carbon as Anodes for Potassium-Ion Batteries. *Advanced Energy Materials* 2018, ***8*** (29).
4. J. Zhou; L. Wang; M. Yang; J. Wu; F. Chen; W. Huang; N. Han; H. Ye; F. Zhao; Y. Li; Y. Li, Hierarchical $VS_2$ Nanosheet Assemblies: A Universal Host Material for the Reversible Storage of Alkali Metal Ions. *Adv Mater* 2017, ***29*** (35).
5. H. Lin; M. Li; X. Yang; D. Yu; Y. Zeng; C. Wang; G. Chen; F. Du, Nanosheets-Assembled CuSe Crystal Pillar as a Stable and High-Power Anode for Sodium-Ion and Potassium-Ion Batteries. *Advanced Energy Materials* 2019, ***9*** (20).
6. D.-S. Bin; S.-Y. Duan; X.-J. Lin; L. Liu; Y. Liu; Y.-S. Xu; Y.-G. Sun; X.-S. Tao; A.-M. Cao; L.-J. Wan, Structural engineering of $SnS_2$/Graphene nanocomposite for high-performance K-ion battery anode. *Nano Energy* 2019, ***60***, 912-918.
7. C. Yang; J. Feng; F. Lv; J. Zhou; C. Lin; K. Wang; Y. Zhang; Y. Yang; W. Wang; J. Li; S. Guo, Metallic Graphene-Like $VSe_2$ Ultrathin Nanosheets: Superior Potassium-Ion Storage and Their Working Mechanism. *Adv Mater* 2018, ***30*** (27), e1800036.
8. J. Xie; Y. Zhu; N. Zhuang; H. Lei; W. Zhu; Y. Fu; M. S. Javed; J. Li; W. Mai, Rational design of metal organic framework-derived $FeS_2$ hollow nanocages@reduced graphene oxide for K-ion storage. *Nanoscale* 2018, ***10*** (36), 17092-17098.
9. M. Mao; C. Cui; M. Wu; M. Zhang; T. Gao; X. Fan; J. Chen; T. Wang; J. Ma; C. Wang, Flexible $ReS_2$ nanosheets/N-doped carbon nanofibers-based paper as a universal anode for alkali (Li, Na, K) ion battery. *Nano Energy* 2018, ***45***, 346-352.
10. R. Hu; K. Zhu; K. Ye; J. Yan; Q. Wang; D. Cao; G. Wang, Influence of potential range selection on the SnS@C/rGO anodes in potassium ion battery. *Appl. Surf. Sci.* 2021, ***536***.
11. Z. Xia; X. Chen; H. Ci; Z. Fan; Y. Yi; W. Yin; N. Wei; J. Cai; Y. Zhang; J. Sun, Designing N-doped graphene/$ReSe_2$/$Ti_3C_2$ MXene heterostructure frameworks as promising anodes for high-rate potassium-ion batteries. *Journal of Energy Chemistry* 2021, ***53***, 155-162.
12. S. Chong; X. Wei; Y. Wu; L. Sun; C. Shu; Q. Lu; Y. Hu; G. Cao; W. Huang, Expanded $MoSe_2$ Nanosheets Vertically Bonded on Reduced Graphene Oxide for Sodium and Potassium-Ion Storage. *ACS Appl. Mater. Interfaces* 2021, ***13*** (11), 13158-13169.